Physica A 442 (2016) 510–522

Contents lists available at ScienceDirect

Physica A

journal homepage: www.elsevier.com/locate/physa

A practical numerical scheme for the ternary Cahn–Hilliard system with a logarithmic free energy

Darae Jeong, Junseok Kim *

Department of Mathematics, Korea University, Seoul 136-713, Republic of Korea

HIGHLIGHTS

- We consider the ternary Cahn–Hilliard system with a logarithmic free energy.
- We regularize the logarithmic function near zero by using a quadratic polynomial.
- The numerical scheme is based on a linear unconditionally gradient stable scheme.
- We show that numerical solutions are stable with practically large enough time steps.

ARTICLE INFO

Article history:
Received 25 February 2015
Received in revised form 3 August 2015
Available online 25 September 2015

Keywords:
Ternary Cahn–Hilliard
Logarithmic free energy
Multigrid method
Phase separation
Finite difference method

ABSTRACT

We consider a practically stable finite difference method for the ternary Cahn–Hilliard system with a logarithmic free energy modeling the phase separation of a three-component mixture. The numerical scheme is based on a linear unconditionally gradient stable scheme by Eyre and is solved by an efficient and accurate multigrid method. The logarithmic function has a singularity at zero. To remove the singularity, we regularize the function near zero by using a quadratic polynomial approximation. We perform a convergence test, a linear stability analysis, and a robustness test of the ternary Cahn–Hilliard equation. We observe that our numerical solutions are convergent, consistent with the exact solutions of linear stability analysis, and stable with practically large enough time steps. Using the proposed numerical scheme, we also study the temporal evolution of morphology patterns during phase separation in one-, two-, and three-dimensional spaces.

1. Introduction

In this paper, we consider an efficient and accurate numerical method of a model for phase separation in a three-component mixture. When a homogeneous system composed of three-components, at high temperature, is rapidly cooled to a uniform temperature θ below a critical temperature θ_c, where it is unstable with respect to concentration fluctuations, spinodal decomposition takes place. The system separates into spatial regions rich in one component and poor in the other components [1]. An understanding of the pattern formation process is practically important because the techniques to solidify materials can influence long-term physical properties of the material [2]. The governing equation is the ternary Cahn–Hilliard (CH) equation [3,4], which is a multicomponent extension of the binary CH equation [5]. For more details on the physical, mathematical, and numerical derivations for the binary CH equation, see the review paper [6] and references therein.

* Corresponding author. Tel.: +82 2 3290 3077; fax: +82 2 929 8562.
E-mail address: cfdkim@korea.ac.kr (J. Kim).
URL: http://math.korea.ac.kr/~cfdkim (J. Kim).

http://dx.doi.org/10.1016/j.physa.2015.09.038
0378-4371/

Let $c_i = c_i(\mathbf{x}, t)$ for $i = 1, 2, 3$ be the mole fraction of the ith component in the mixture as a function of space ($\mathbf{x}$) and time (t). Since the sum of mole fractions is 1, we only need to solve the governing equations for c_1 and c_2. We consider the following ternary CH system with a logarithmic free energy [1]:

$$\frac{\partial c_1}{\partial t} = \Delta \mu_1, \quad \mathbf{x} \in \Omega, \ t > 0, \tag{1}$$

$$\mu_1 = \theta \ln(c_1) - \theta_c c_1 - \epsilon^2 \Delta c_1 - \frac{\theta}{3} \ln[c_1 c_2 (1 - c_1 - c_2)], \tag{2}$$

$$\frac{\partial c_2}{\partial t} = \Delta \mu_2, \tag{3}$$

$$\mu_2 = \theta \ln(c_2) - \theta_c c_2 - \epsilon^2 \Delta c_2 - \frac{\theta}{3} \ln[c_1 c_2 (1 - c_1 - c_2)], \tag{4}$$

where Ω is an open domain in $\mathbb{R}^d$ ($d = 1, 2, 3$) and ϵ is the gradient energy coefficient. The mass conserving and natural boundary conditions for the system are $\nabla \mu_i \cdot \mathbf{n} = 0$ and $\nabla c_i \cdot \mathbf{n} = 0$ on $\partial\Omega$, respectively. Here, $\mathbf{n}$ is the unit normal vector to $\partial\Omega$. The governing Eqs. (1)–(4) can be derived from a Ginzburg–Landau free energy functional $\mathcal{E}$ [7]:

$$\mathcal{E}(t) = \int_\Omega \sum_{i=1}^{3} \left(\theta c_i \ln c_i + \theta_c c_i c_{\mathrm{mod}(i,3)+1} + \frac{\epsilon^2}{2} |\nabla c_i|^2 \right) d\mathbf{x}. \tag{5}$$

Authors in Ref. [8] proved existence, uniqueness, and stability of the fully implicit finite-element approximation for a sufficiently small time step. The non-linear Gauss–Seidel-type iteration is used for the implicit finite element approximation and has a time step constraint ($\Delta t = O(\epsilon^2) = O(h^2)$). In Ref. [1], an explicit finite element is used and has a severe time step constraint ($\Delta t = O(h^4)$). To avoid these time step constraints associated with a logarithmic free energy, a polynomial type free energy is used [9,10]. Authors in Refs. [11–13] have studied an unconditionally stable scheme to the ternary CH system with polynomial free energy. See Ref. [14] for the hierarchy of consistent n-component CH systems. However, to the authors' knowledge, there has been no trial to apply an unconditionally stable scheme to a ternary CH system with a logarithmic free energy in the context of the finite difference method. The purpose of this work is to propose a conservative and robust numerical method for the ternary CH system with a thermodynamically consistent logarithmic free energy for a three-component mixture.

The contents of this paper are as follows. In Section 2, we consider a fully discrete semi-implicit finite difference scheme for the ternary CH system. We present numerical experiments such as a convergence test, linear stability analysis of the equations, a robustness test, and phase separation in a ternary mixture in Section 3. Finally, conclusions are drawn in Section 4.

2. Numerical solution

Since $c_3 = 1 - c_1 - c_2$ for three-component systems, we only need to solve the equations with c_1 and c_2. In the following numerical scheme and solution algorithm, we restrict ourselves to one-dimensional space for simplicity. The extension of two-dimensional problem is straightforward. We discretize the ternary CH equation in one-dimensional space $\Omega = (a, b)$. Let N be a positive even integer, $h = (b - a)/N$ be the uniform mesh size, $\Omega_h = \{x_i | x_i = (i - 0.5)h, \ 1 \le i \le N\}$ be the set of cell-centers, and Δt be the time step. For simplicity of notations, let $\phi = c_1$, $\mu = \mu_1$, $\psi = c_2$, and $\nu = \mu_2$. Let ϕ_i^n, ψ_i^n, μ_i^n, and ν_i^n be approximations of $\phi(x_i, n\Delta t)$, $\psi(x_i, n\Delta t)$, $\mu(x_i, n\Delta t)$, and $\nu(x_i, n\Delta t)$, respectively. To avoid a numerical difficulty in dealing with a singularity at zero, we apply a regularization to the logarithmic function, i.e., for small positive number δ, we define

$$\ln_\delta(\phi) := \begin{cases} \ln(\phi), & \text{if } \phi \ge \delta, \\ p(\phi) = -\dfrac{1}{2\delta^2}\phi^2 + \dfrac{2}{\delta}\phi + \ln(\delta) - \dfrac{3}{2}, & \text{otherwise,} \end{cases}$$

where the quadratic polynomial $p(\phi)$ matches the values of zero, first, and second derivatives of the logarithmic function at $\phi = \delta$. The ideas of regularizing of the logarithmic free energy for the binary and multi-component cases were stated by Barrett and Blowey [15,16].

To propose a robust numerical method, we use the idea of the convex splitting scheme developed by Eyre [17]. The general idea, in the context of a reaction–diffusion equation, was introduced in Elliott and Stuart [18], see Eq. (5.4) therein. Barrett and Blowey [19,20] also developed the idea in the context of the multi-component CH system with the deep quench limit ($\theta \to 0$) and the multi-component CH system with a logarithmic free energy. Moreover, Barrett and Blowey [20] suggested that a two level scheme with the convex splitting version is unconditionally stable.

In this paper, we propose a practically stable scheme for Eqs. (1)–(4):

$$\frac{\phi_i^{n+1} - \phi_i^n}{\Delta t} = \Delta_h \mu_i^{n+1}, \tag{6}$$

$$\mu_i^{n+1} = \theta \ln_\delta(\phi_i^n) - (s+1)\theta_c\phi_i^n + s\theta_c\phi_i^{n+1} - \epsilon^2\Delta_h\phi_i^{n+1} - \frac{\theta}{3}[\ln_\delta(\phi_i^n) + \ln_\delta(\psi_i^n) + \ln_\delta(1-\phi_i^n-\psi_i^n)], \quad (7)$$

$$\frac{\psi_i^{n+1}-\psi_i^n}{\Delta t} = \Delta_h\nu_i^{n+1}, \quad (8)$$

$$\nu_i^{n+1} = \theta \ln_\delta(\psi_i^n) - (s+1)\theta_c\psi_i^n + s\theta_c\psi_i^{n+1} - \epsilon^2\Delta_h\psi_i^{n+1} - \frac{\theta}{3}[\ln_\delta(\phi_i^n) + \ln_\delta(\psi_i^n) + \ln_\delta(1-\phi_i^n-\psi_i^n)], \quad (9)$$

where s is a non-negative number and $\Delta_h\phi_i = (\phi_{i-1} - 2\phi_i + \phi_{i+1})/h^2$. In the right hand side of Eq. (7), $\theta \ln_\delta(\phi^n) - (s+1)\theta_c\phi^n + s\theta_c\phi^{n+1}$ can be rewritten as $F_c'(\phi^{n+1}) - F_e'(\phi^n)$, where $F_c(\phi) = 0.5s\theta_c\phi^2$ is a contractive term and $F_e(\phi) = 0.5(s+1)\theta_c\phi^2 - \theta\phi\ln_\delta(\phi) + \theta\phi$ is an expansive term.

Note that both functions $F_c(\phi)$ and $F_e(\phi)$ are strictly convex in the region satisfying

$$\phi > \begin{cases} \dfrac{\theta}{(s+1)\theta_c}, & \text{if } \phi \geq \delta, \\ \dfrac{4\delta\theta - (s+1)\theta_c\delta^2}{3\theta}, & \text{otherwise.} \end{cases} \quad (10)$$

Also, we can consider this convex splitting scheme as a numerical dissipation term of type $F_c'(\phi^{n+1}) - F_e'(\phi^n) = \theta\ln_\delta(\phi^n) - \theta_c\phi^n + s\theta_c\Delta t(\phi^{n+1}-\phi^n)/\Delta t$. The key novelty in this paper is that the scheme leads to a linear system at each time level, and is stable when the parameter s is chosen to satisfying (10) with $\phi = \phi_i^n$ for all $i = 1, \ldots, N$ and $n \geq 1$.

At the boundary, the homogeneous Neumann condition is implemented as

$$\nabla_h\phi^n_{\frac{1}{2}} = \nabla_h\phi^n_{N+\frac{1}{2}} = \nabla_h\mu^n_{\frac{1}{2}} = \nabla_h\mu^n_{N+\frac{1}{2}} = 0,$$
$$\nabla_h\psi^n_{\frac{1}{2}} = \nabla_h\psi^n_{N+\frac{1}{2}} = \nabla_h\nu^n_{\frac{1}{2}} = \nabla_h\nu^n_{N+\frac{1}{2}} = 0,$$

where $\nabla_h\phi^n_{i+\frac{1}{2}} = (\phi^n_{i+1} - \phi^n_i)/h$. We define a discrete energy functional as

$$\begin{aligned} \mathcal{E}^h(\phi^n, \psi^n) = h\sum_{i=1}^{N} & \theta\left[\phi_i^n\ln\phi_i^n + \psi_i^n\ln\psi_i^n + (1-\phi_i^n-\psi_i^n)\ln(1-\phi_i^n-\psi_i^n)\right] \\ & + \theta_c[\phi_i^n\psi_i^n + (\phi_i^n+\psi_i^n)(1-\phi_i^n-\psi_i^n)] \\ & + \frac{\epsilon^2 h}{2}\sum_{i=1}^{N-1}\left(\left|\nabla_h\phi^n_{i+\frac{1}{2}}\right|^2 + \left|\nabla_h\psi^n_{i+\frac{1}{2}}\right|^2 + \left|\nabla_h\phi^n_{i+\frac{1}{2}} + \nabla_h\psi^n_{i+\frac{1}{2}}\right|^2\right). \end{aligned} \quad (11)$$

We apply a multigrid method to solve the system of discrete Eqs. (6)–(9). Instead of solving the four Eqs. (6)–(9) at the same time, with given ϕ^n and ψ^n, we sequentially solve Eqs. (6) and (7), and then solve Eqs. (8) and (9). See more details in Refs. [12,21]. For simplicity of exposition, we only describe the linear multigrid method for Eqs. (6) and (7). First, let us rewrite Eqs. (6) and (7) as follows.

$$\mathcal{L}(\phi_i^{n+1}, \mu_i^{n+1}) = (f_i^n, g_i^n), \quad (12)$$

where the linear operator $\mathcal{L}$ is defined as

$$\mathcal{L}(\phi_i^{n+1}, \mu_i^{n+1}) = \left(\phi_i^{n+1}/\Delta t - \Delta_h\mu_i^{n+1},\ \mu_i^{n+1} - s\theta_c\phi_i^{n+1} + \epsilon^2\Delta_h\phi_i^{n+1}\right)$$

and the source term is denoted by

$$\left(f_i^n, g_i^n\right) = \left(\frac{\phi_i^n}{\Delta t},\ \theta\ln_\delta(\phi_i^n) - (s+1)\theta_c\phi_i^n - \frac{\theta}{3}\left[\ln_\delta(\phi_i^n) + \ln_\delta(\psi_i^n) + \ln_\delta(1-\phi_i^n-\psi_i^n)\right]\right)$$

for $i = 1, \ldots, N$. Next, we describe the linear multigrid method, which includes the presmoothing, coarse grid correction, and postsmoothing steps. See the Refs. [22,23] for additional details and background of the linear multigrid method.

We denote a mesh grid Ω_k as the discrete domain for each multigrid level k, that is,

$$\Omega_k = \{x_i = (i-0.5)h_k \mid 1 \leq i \leq 2^{k+1} \text{ and } h_k = 2^{K-k}h\}.$$

Note that K means the finest grid level and satisfies $N = p\cdot 2^K$, where p is odd number. For $k = K, \ldots, 1$, we define the successively coarser grids.

We now introduce the algorithm of the linear multigrid iteration for solving the discretized Eq. (12) on grid Ω_k.

$$\{\boldsymbol{\phi}_k^{n+1,m+1}, \boldsymbol{\mu}_k^{n+1,m+1}\} = MGcycle(k, \boldsymbol{\phi}_k^{n+1,m}, \boldsymbol{\mu}_k^{n+1,m}, \mathcal{L}_k, \boldsymbol{f}_k, \boldsymbol{g}_k, \alpha).$$

Here, $\{\boldsymbol{\phi}_k^{n+1,m}, \boldsymbol{\mu}_k^{n+1,m}\}$ and $\{\boldsymbol{\phi}_k^{n+1,m+1}, \boldsymbol{\mu}_k^{n+1,m+1}\}$ are the approximations of $\boldsymbol{\phi}^{n+1}$ and $\boldsymbol{\mu}^{n+1}$ before and after a multigrid cycle on grid level k. And the bold letter means the vector. For example, $\boldsymbol{\phi}_k$ denotes $\boldsymbol{\phi}_k = (\phi_1, \phi_2, \ldots, \phi_{2^{k+1}})$. By starting from initial values $\boldsymbol{\phi}^{n+1,0} = \boldsymbol{\phi}^n$ and $\boldsymbol{\mu}^{n+1,0} = \boldsymbol{\mu}^n$, one step of the iteration is given in the following step:

Step (1) *Presmoothing*

$$\{\bar{\boldsymbol{\phi}}_k^{n+1,m},\ \bar{\boldsymbol{\mu}}_k^{n+1,m}\} = SMOOTH^{\alpha}(\boldsymbol{\phi}_k^{n+1,m}, \boldsymbol{\mu}_k^{n+1,m}, \mathcal{L}_k, \boldsymbol{f}_k^n, \boldsymbol{g}_k^n),$$

which means performing α smoothing steps with the initial approximations $\boldsymbol{\phi}_k^{n+1,m}$, $\boldsymbol{\mu}_k^{n+1,m}$, source terms $\boldsymbol{f}_k^n, \boldsymbol{g}_k^n$, and *SMOOTH* relaxation operator to get the approximations $\bar{\boldsymbol{\phi}}_k^{n+1,m}$, $\bar{\boldsymbol{\mu}}_k^{n+1,m}$. By applying Gauss–Seidel iteration, we have the following smoothing (relaxation) step for Eqs. (6) and (7):

$$\frac{\phi_i^{n+1,m,s+1}}{\Delta t} + \frac{2\mu_i^{n+1,m,s+1}}{h^2} = f_i^n + \frac{\mu_{i-1}^{n+1,m,s+1} + \mu_{i+1}^{n+1,m,s}}{h^2}, \tag{13}$$

$$-\left(s\theta_c + \frac{2\epsilon^2}{h^2}\right)\phi_i^{n+1,m,s+1} + \mu_i^{n+1,m,s+1} = g_i^n - \epsilon^2\frac{\phi_{i-1}^{n+1,m,s+1} + \phi_{i+1}^{n+1,m,s}}{h^2}, \quad \text{for } i = 1, 2, \ldots, 2^{k+1}. \tag{14}$$

Here, we denote $\phi_i^{n+1,m,s}$ and $\phi_i^{n+1,m,s+1}$ as current and the new approximations in a Gauss–Seidel iteration. One *SMOOTH* relaxation operator step consists of solving the system (13) and (14) given below by 2×2 matrix inversion for each i. After taking α smoothing steps, we have $\bar{\boldsymbol{\phi}}_k^{n+1,m}$ and $\bar{\boldsymbol{\mu}}_k^{n+1,m}$.

Step (2) *Compute the residual*

$$(\bar{\mathbf{d}}_{1k}^{\,m}, \bar{\mathbf{d}}_{2k}^{\,m}) = (\mathbf{f}_k^n, \mathbf{g}_k^n) - \mathcal{L}_k(\bar{\boldsymbol{\phi}}_k^{n+1,m}, \bar{\boldsymbol{\mu}}_k^{n+1,m}). \tag{15}$$

Step (3) *Restrict the residual*

$$(\bar{\mathbf{d}}_{1k-1}^{\,m}, \bar{\mathbf{d}}_{2k-1}^{\,m}) = I_k^{k-1}(\bar{\mathbf{d}}_{1k}^{\,m}, \bar{\mathbf{d}}_{2k}^{\,m}),$$

where the restriction operator I_k^{k-1} maps k-level functions to $(k-1)$-level functions. The components of $\bar{\mathbf{d}}_{k-1}^m$ are given by

$$\bar{\mathbf{d}}_{k-1}^m(x_{2i}) = \left(\bar{\mathbf{d}}_k^m(x_i) + \bar{\mathbf{d}}_k^m(x_{i+1})\right)/2$$

for $i = 1, 2, \ldots, 2^k$.

Step (4) *Compute an approximation* $\{\hat{\boldsymbol{v}}_{k-1}^{n+1,m},\ \hat{\boldsymbol{w}}_{k-1}^{n+1,m}\}$ on Ω_{k-1}.

If $k > 1$, we perform a *MGcycle* with an initial guess as

$$\{\hat{\boldsymbol{v}}_{k-1}^m, \hat{\boldsymbol{w}}_{k-1}^m\} = MGcycle(k-1, \mathbf{0}, \mathbf{0}, \mathcal{L}_{k-1}, \bar{\mathbf{d}}_{1k-1}^{\,m}, \bar{\mathbf{d}}_{2k-1}^{\,m}, \alpha).$$

If $k = 1$, we relax α times on $\mathcal{L}(\boldsymbol{\phi}^{n+1}, \boldsymbol{\mu}^{n+1}) = (\boldsymbol{f}^n, \boldsymbol{g}^n)$.

$$\{\hat{\boldsymbol{v}}_{k-1}^m,\ \hat{\boldsymbol{w}}_{k-1}^m\} = SMOOTH^{\alpha}(\mathbf{0}, \mathbf{0}, \mathcal{L}_{k-1}, \bar{\mathbf{d}}_{1k-1}^{\,m}, \bar{\mathbf{d}}_{2k-1}^{\,m}).$$

Step (5) *Interpolate the correction*

$$(\hat{\boldsymbol{v}}_k^m, \hat{\boldsymbol{w}}_k^m) = I_{k-1}^k(\hat{\boldsymbol{v}}_{k-1}^m, \hat{\boldsymbol{w}}_{k-1}^m).$$

Here, the coarse values are simply transferred to the two nearby fine grid points, i.e. $\boldsymbol{v}_k(x_{2i}) = \boldsymbol{v}_k(x_{2i-1}) = \boldsymbol{v}_{k-1}(x_i)$ for $i = 1, 2, \ldots, 2^k$.

Step (6) *Compute the corrected approximation on* Ω_k

$$\boldsymbol{\phi}_k^{m,\text{after CGC}} = \bar{\boldsymbol{\phi}}_k^m + \hat{\boldsymbol{v}}_k^m, \qquad \boldsymbol{\mu}_k^{m,\text{after CGC}} = \bar{\boldsymbol{\mu}}_k^m + \hat{\boldsymbol{w}}_k^m.$$

Step (7) *Postsmoothing*

$$\{\boldsymbol{\phi}_k^{n+1,m+1}, \boldsymbol{\mu}_k^{n+1,m+1}\} = SMOOTH^{\nu}(\boldsymbol{\phi}_k^{m,\text{after CGC}}, \boldsymbol{\mu}_k^{m,\text{after CGC}}, \mathcal{L}_k, \boldsymbol{f}_k^n, \boldsymbol{g}_k^n).$$

This completes the description of a *MGcycle*. One *MGcycle* step stops if the consecutive error $|\boldsymbol{\phi}_k^{n+1,m+1} - \boldsymbol{\phi}_k^{n+1,m}|$ is smaller than a given tolerance *tol*. Similarly, we use the linear multigrid method for Eqs. (8) and (9).

3. Numerical experiments

In this section, we perform numerical experiments such as a convergence test, a linear stability analysis, and phase separation in a three component mixture. Unless otherwise specified, we will use $\theta_c = 1$ and $\theta = 0.3$. Then, the three minima of $\sum_{i=1}^3 \left(\theta c_i \ln c_i + \theta_c c_i c_{\text{mod}(i,3)+1}\right)$ are approximately at (0.0550533, 0.0550533, 0.8898934), the other two values being permutations.

From the condition (10), we obtain the s which satisfying that $F_e(\phi)$ is strictly convex as follows:

$$\phi \geq \min(\phi) \approx 0.0550533 > \frac{\theta}{(s+1)\theta_c} = \frac{0.3}{(s+1)}.$$

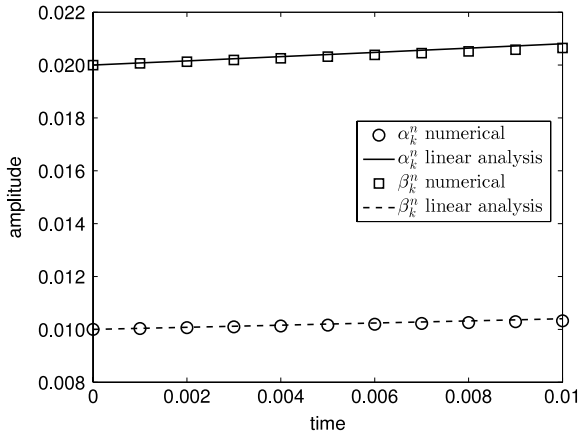

Fig. 1. Temporal evolution of the numerical amplitudes $\alpha_k(t)$, $\beta_k(t)$, and its corresponding results by linear stability analysis.

Table 1
l_2-error and convergence rate for ϕ and ψ.

N_x	64	Rate	128	Rate	256	Rate	512
ϕ	1.0039e−5	1.9469	2.6039e−6	1.9765	6.6164e−7	1.9554	1.7060e−7
ψ	1.6176e−5	1.9470	4.1955e−6	1.9815	1.0624e−6	1.9762	2.7003e−7

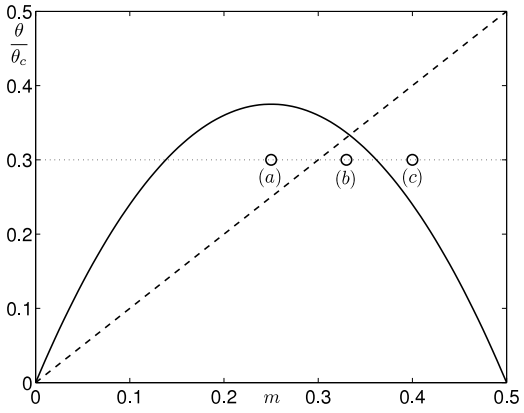

Fig. 2. Instability curve with θ/θ_c against m when $\theta_c = 1$.

Therefore, we have the condition $s > 4.4493\cdots$. In all numerical tests, we take $s = 5$. Also, we use $\delta = 0.001$ from the smallest value of the three minima.

3.1. Convergence test

To verify the accuracy of the numerical scheme, we perform the convergence test. In this test, the initial conditions are

$$\phi(x, 0) = 0.4 - 0.01\cos(2\pi x), \qquad \psi(x, 0) = 0.2 - 0.01\cos(2\pi x)$$

on a domain $\Omega = (0, 1)$. The numerical solutions are computed up to time $T = 3.90625\text{e}-3$ on the uniform grids, $h = 1/2^n$, and with corresponding time steps, $\Delta t = h^2$ for $n = 6, 7, 8$, and 9. And we use $\epsilon = 0.1$. Since there is no closed-form of analytical solution for this problem, we consider a reference numerical solution, ϕ^{ref}, which is obtained with very fine spatial and temporal grids. In this test, we use $h = 1/2048$ and $\Delta t = 1/2048^2$ for the reference solution. Then we denote the error by $e := \phi - \phi^{\text{ref}}$. The convergence rate is defined as the ratio of successive errors, $\log_2(\|e_h\|/\|e_{\frac{h}{2}}\|)$. Here, $\|e_h\|$ is measured by the discrete l_2-norm of the error e_h. Table 1 lists the discrete l_2-norm of errors and convergence rates for ϕ and ψ. The results suggest that the proposed numerical scheme is first and second order accurate in time and space, respectively.

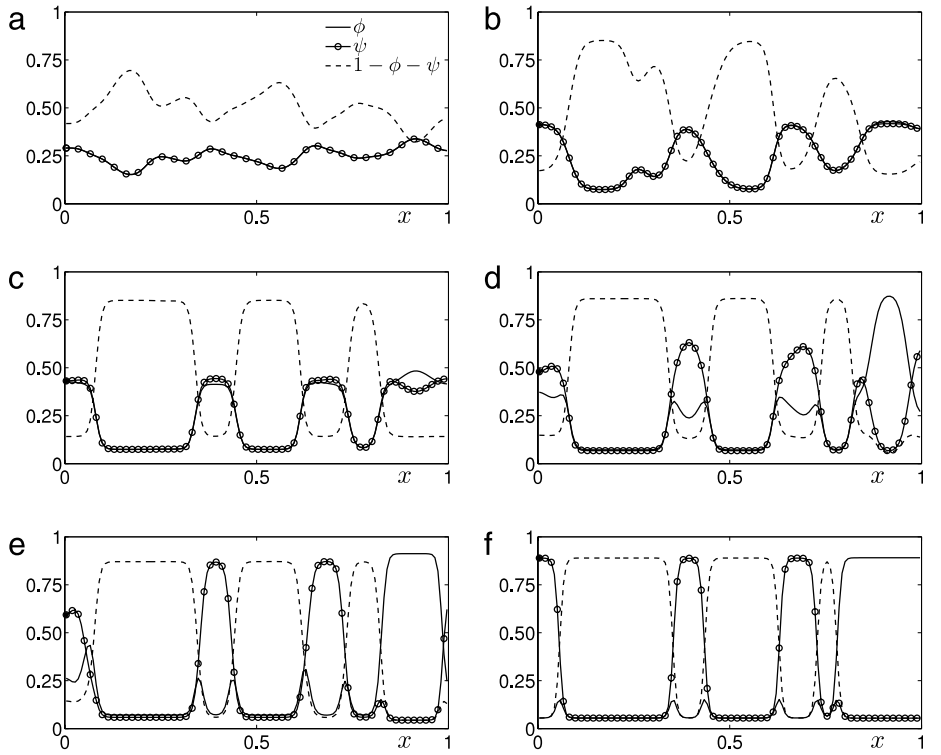

Fig. 3. (a)–(f) Temporal evolution of a ternary system with average concentrations $(m_1, m_2) = (0.25, 0.25)$ at time $t = 10$, 15, 20, 25, 30, and 100, respectively.

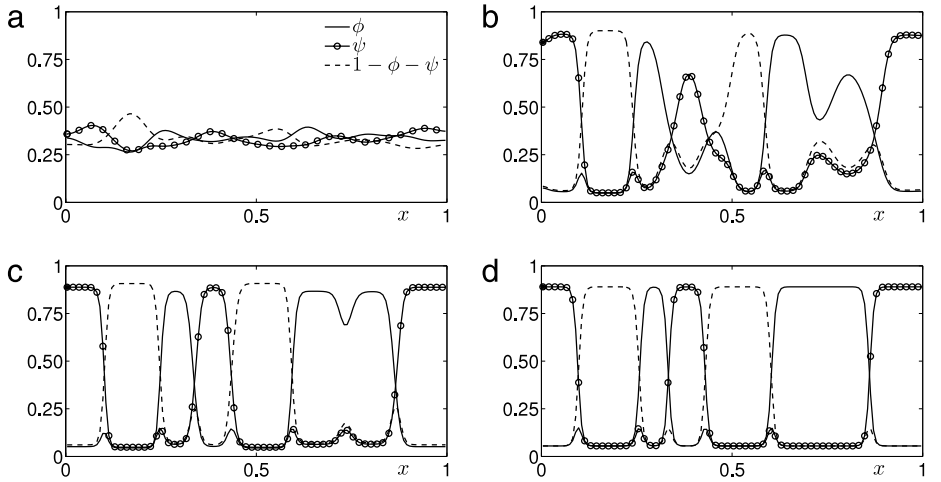

Fig. 4. (a)–(d) Temporal evolution of a ternary system with average concentrations $(m_1, m_2) = (1/3, 1/3)$ at time $t = 15$, 25, 30, and 100, respectively.

3.2. Linear stability analysis

Let the mean concentration take the form $\mathbf{m} = (m_1, m_2, m_3)$. Here, m_1, m_2, and m_3 are positive and $m_3 = 1 - m_1 - m_2$. We assume that $m = m_1 = m_2$ and we seek a solution of the form

$$\begin{pmatrix} \phi(x,t) \\ \psi(x,t) \end{pmatrix} = \begin{pmatrix} m \\ m \end{pmatrix} + \sum_{k=1}^{\infty} \begin{pmatrix} \alpha_k(t)\cos(k\pi x) \\ \beta_k(t)\cos(k\pi x) \end{pmatrix}, \tag{16}$$

where $|\alpha_k(t)|, |\beta_k(t)| \ll 1$ [8]. After linearizing the nonlinear terms in Eqs. (1)–(4) about $(m, m, 1-2m)$, we have

$$\frac{\partial \phi}{\partial t} = \Delta\mu, \tag{17}$$

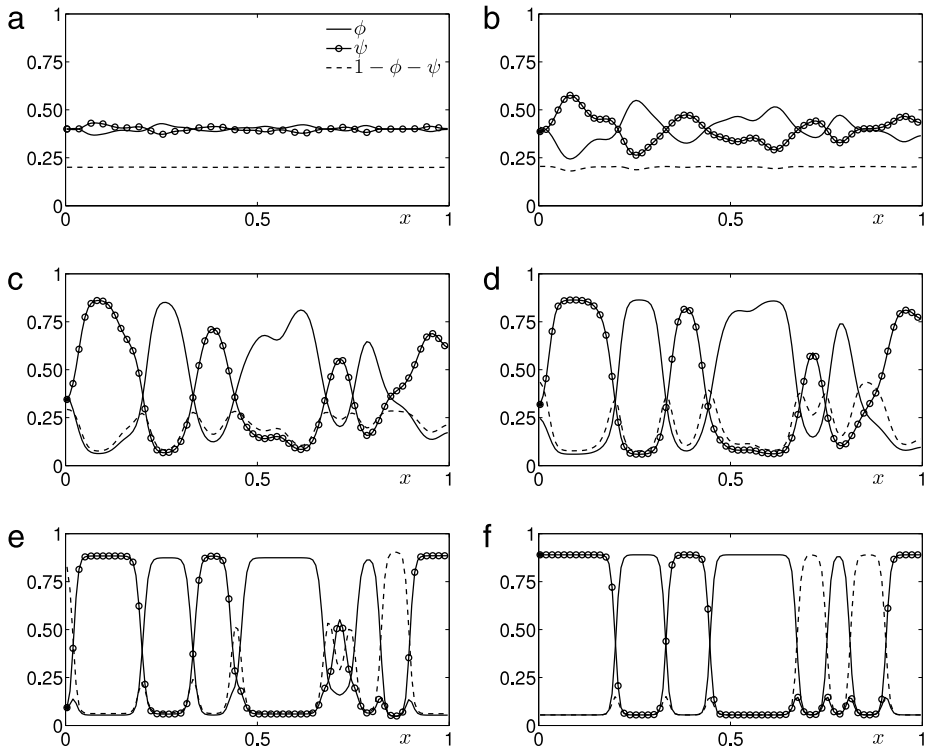

Fig. 5. (a)–(f) Temporal evolution of a ternary system with average concentrations $(m_1, m_2) = (0.4, 0.4)$ at time $t = 4, 8, 12, 14, 20$, and 100, respectively.

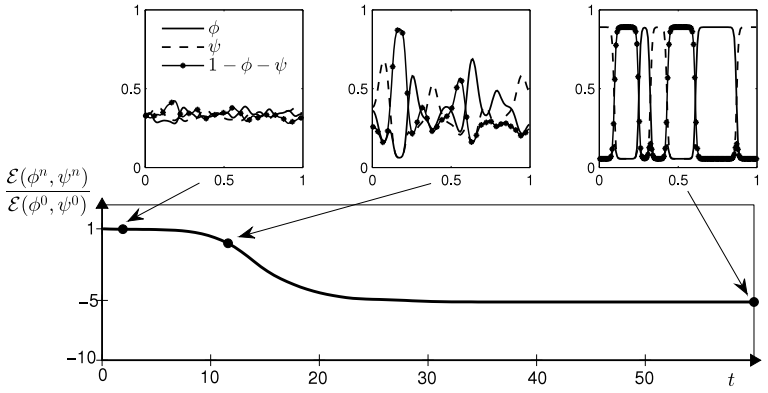

Fig. 6. Normalized discrete energy dissipation and temporal profiles of ϕ, ψ, and $1-\phi-\psi$ at time $t = 4$, 12, and 60, respectively.

$$\mu = \theta \ln(m) + \frac{\theta(\phi - m)}{m} - \theta_c \phi - \epsilon^2 \Delta\phi - \frac{\theta}{3}\left(\ln[m^2(1-2m)] + \frac{(1-3m)(\phi - m)}{m(1-2m)} + \frac{(1-3m)(\psi - m)}{m(1-2m)}\right), \quad (18)$$

$$\frac{\partial \psi}{\partial t} = \Delta \nu, \quad (19)$$

$$\nu = \theta \ln(m) + \frac{\theta(\psi - m)}{m} - \theta_c \psi - \epsilon^2 \Delta\psi - \frac{\theta}{3}\left(\ln[m^2(1-2m)] + \frac{(1-3m)(\phi - m)}{m(1-2m)} + \frac{(1-3m)(\psi - m)}{m(1-2m)}\right). \quad (20)$$

By substituting Eq. (16) into Eqs. (17)–(20), we obtain

$$\begin{pmatrix} \alpha_k'(t) \\ \beta_k'(t) \end{pmatrix} = \mathbf{A} \begin{pmatrix} \alpha_k(t) \\ \beta_k(t) \end{pmatrix}, \quad \text{where } \mathbf{A} = \begin{pmatrix} a & b \\ b & a \end{pmatrix}, \quad (21)$$

$$\text{and } a = -(k\pi)^2 \left[\frac{\theta(2-3m)}{3m(1-2m)} - \theta_c + \epsilon^2 (k\pi)^2\right], \qquad b = \frac{(k\pi)^2 \theta(1-3m)}{3m(1-2m)}.$$

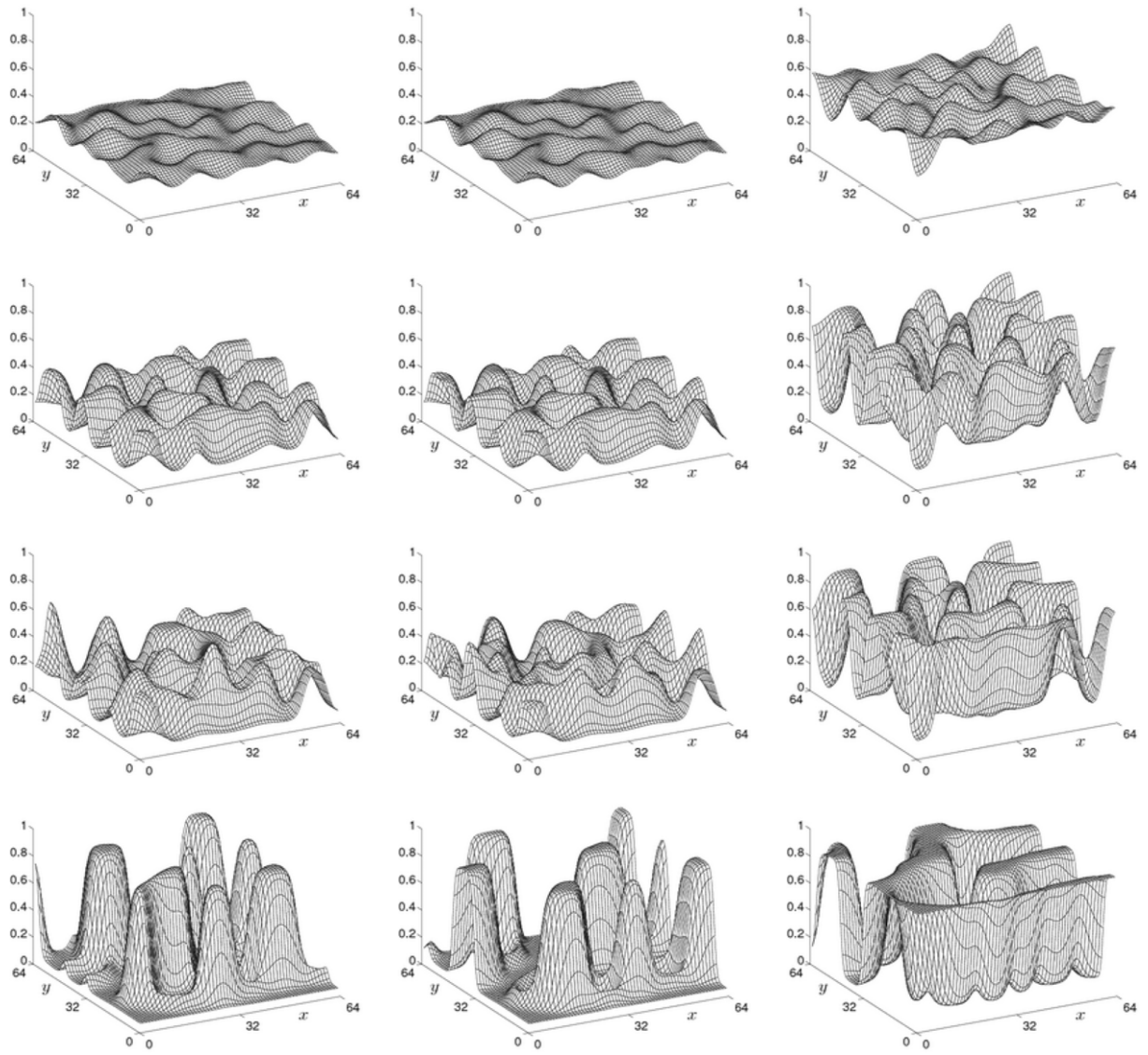

(a) ϕ. (b) ψ. (c) $1-\phi-\psi$.

Fig. 7. Temporal evolution of a ternary system with average concentrations $(m_1, m_2) = (0.25, 0.25)$ at time $t = 200, 400, 600$, and 3000 (from top to bottom).

The eigenvalues of $\mathbf{A}$ are $\lambda_1 = a - b$ and $\lambda_2 = a + b$. The solution to the system of the ordinary differential equations (21) is given by

$$\begin{pmatrix}\alpha_k(t)\\ \beta_k(t)\end{pmatrix} = \frac{e^{\lambda_1 t}}{2}\begin{pmatrix}-\alpha_k(0)+\beta_k(0)\\ \alpha_k(0)-\beta_k(0)\end{pmatrix} + \frac{e^{\lambda_2 t}}{2}\begin{pmatrix}\alpha_k(0)+\beta_k(0)\\ \alpha_k(0)+\beta_k(0)\end{pmatrix}.$$

For the numerical test, we take the initial condition as

$$\phi(x,0) = m + 0.01\cos(k\pi x), \qquad \psi(x,0) = m + 0.02\cos(k\pi x) \quad \text{on } \Omega = (0,1).$$

And the other parameters are $m = 1/3$, $k = 2$, and $\epsilon = 0.00125$. The numerical simulations are run up to $T = n\Delta t = 0.01$ with $\Delta t = 0.001$ and $h = 1/512$. Fig. 1 shows the temporal evolution of the numerical amplitudes $\alpha_k(t)$, $\beta_k(t)$, and its corresponding linear stability analysis results. The results are in good agreement in a linear regime.

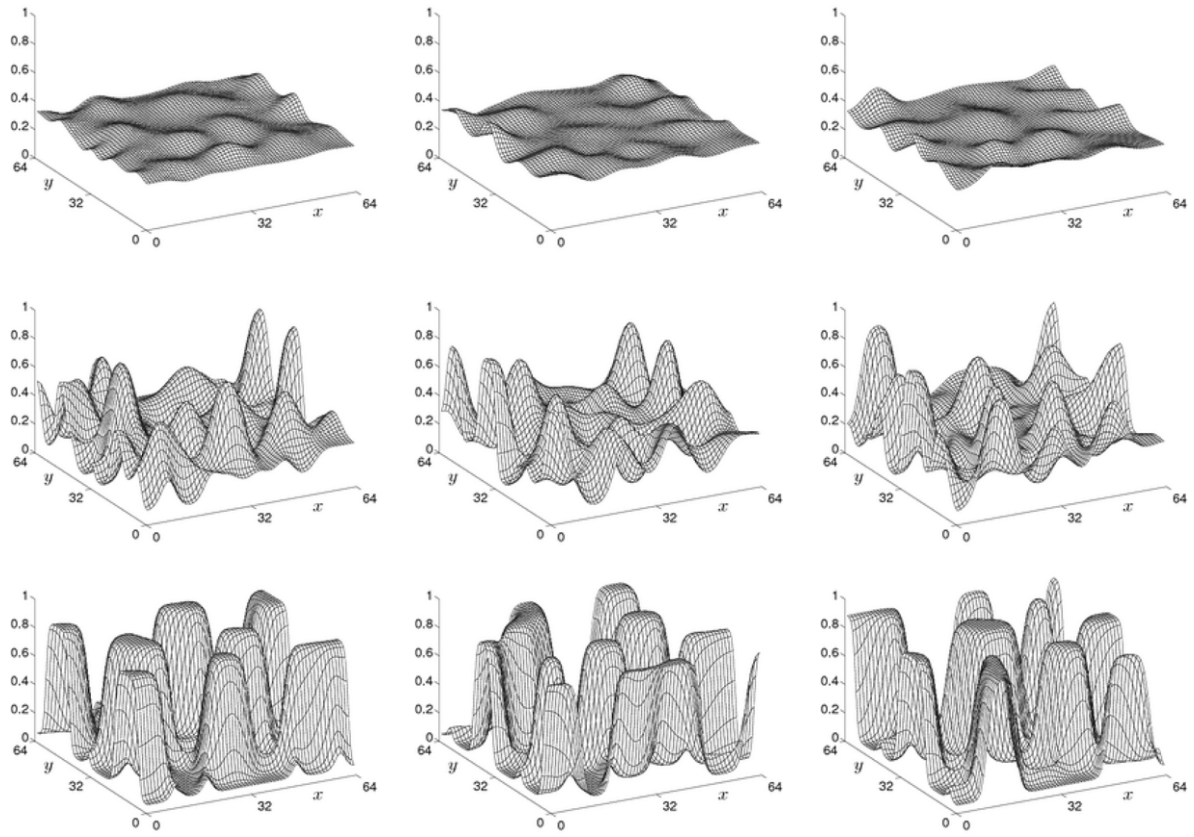

(a) ϕ. (b) ψ. (c) $1-\phi-\psi$.

Fig. 8. Temporal evolution of a ternary system with average concentrations $(m_1, m_2) = (1/3, 1/3)$ at time $t = 500,\ 800$, and 3000 (from top to bottom).

3.3. One-dimensional spinodal decomposition

For small k and ϵ, let us consider the instability curves which determine the definite or indefinite regions. To find these curves, we need to solve the equation $\det \mathbf{A} = 0$ in Eq. (21). In other words, we have to consider $\det \mathbf{A} = a^2 - b^2 = 0$, i.e.,

$$a - b = -(k\pi)^2\left[\theta m - \theta_c + \epsilon^2(k\pi)^2\right] = 0,$$
$$a + b = -(k\pi)^2\left[\frac{\theta}{3m(1-2m)} - \theta_c + \epsilon^2(k\pi)^2\right] = 0.$$

Assuming $\epsilon \to 0$, we have that $\theta/\theta_c = m$ and $\theta/\theta_c = 3m(1-2m)$. For more details, see Ref. [8]. Fig. 2 shows the instability curves when $\phi = \psi = m$ and $\theta_c = 1$. In this figure, the straight profile $\theta/\theta_c = m$ and the parabolic profile $\theta/\theta_c = 3m(1-2m)$ are illustrated by the dashed and solid lines, respectively.

Now, we perform the numerical simulations of spinodal decomposition in ternary system with three points indicated in Fig. 2. Here, (a), (b), and (c) denote $m = 0.25$, $1/3$, and 0.4 when $\theta = 0.3$ and $\theta_c = 1$, respectively. The initial conditions are obtained by random perturbations at the uniform state (m_1, m_2) as

$$\phi(x, 0) = m_1 + 0.05\ \mathrm{rand}(x), \qquad \psi(x, 0) = m_2 + 0.05\ \mathrm{rand}(x),$$

where m_1 and m_2 are the mean concentrations of ϕ and ψ, respectively. The random number $\mathrm{rand}(x)$ is in $[-1, 1]$ and has zero mean. We choose $h = 1/128$, $\Delta t = 0.1$, and $\epsilon = 0.005$ on the interval $\Omega = (0, 1)$.

3.3.1. $m_1 = m_2 = 0.25$

First, we perform the numerical simulation with $m_1 = m_2 = 0.25$, which is point (a) in Fig. 2. Fig. 3 shows the temporal evolution of three compositions. As shown in Fig. 3(a) and (b), ϕ and ψ evolve to the same direction with a two-phase structure. However, after $t = 15$, we see the growth of ϕ and ψ to different direction in Fig. 3(c)–(f) because the composition takes the value of a critical point of the free energy.

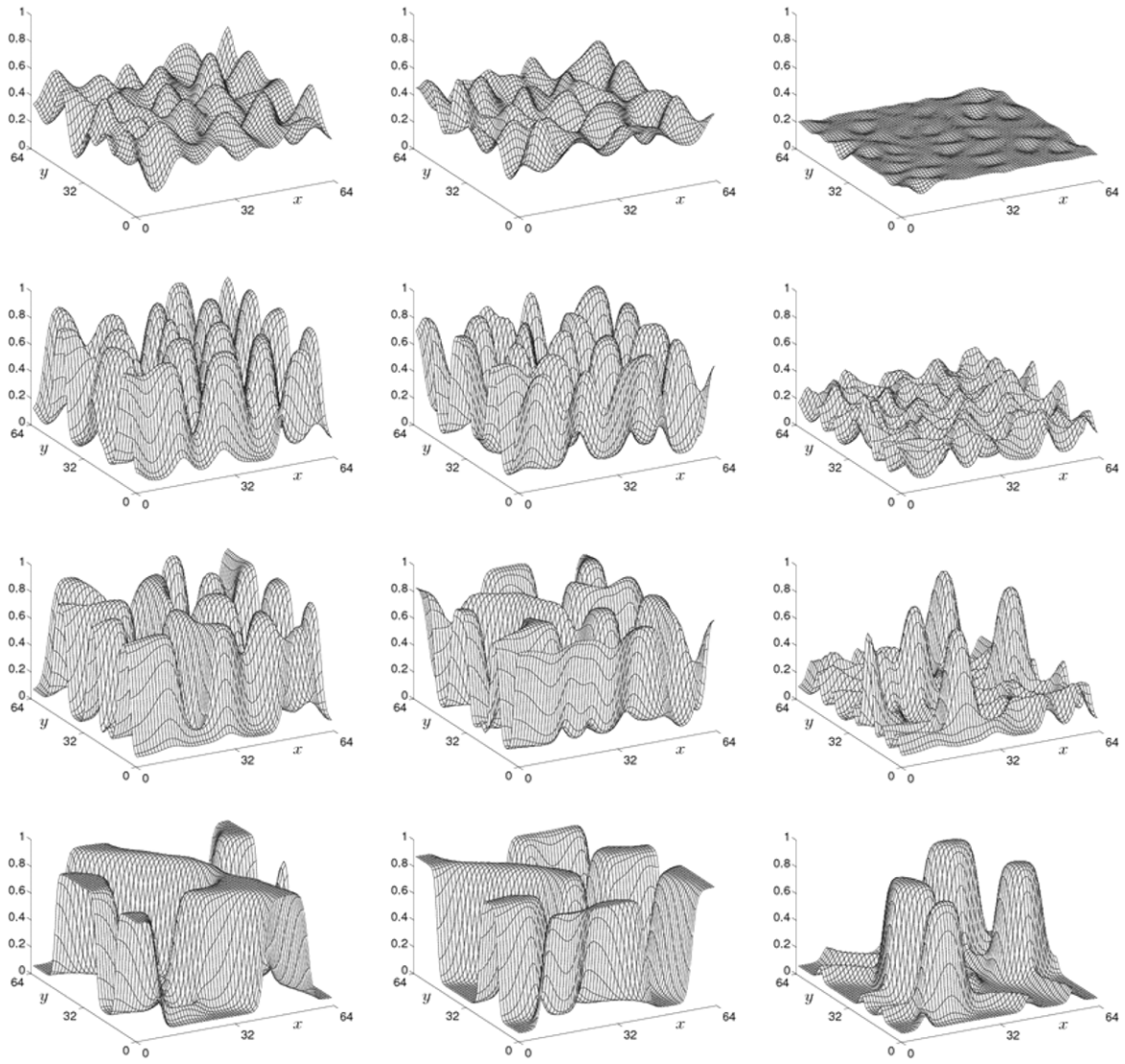

(a) ϕ. (b) ψ. (c) $1-\phi-\psi$.

Fig. 9. Temporal evolution of a ternary system with average concentrations $(m_1, m_2) = (0.4, 0.4)$ at time $t = 200$, 400, 800, and 3000 (from top to bottom).

3.3.2. $m_1 = m_2 = 1/3$

Next, we take $m_1 = m_2 = 1/3$, corresponding to the point (b) in Fig. 2, we show the temporal evolution in Fig. 4. As time goes on, separation of three phases takes place via the spinodal decomposition.

3.3.3. $m_1 = m_2 = 0.4$

In this test, we use $m_1 = m_2 = 0.4$ which is the point (c) in Fig. 2. After quench, two phases dominate by ϕ and ψ. Also, the other phase is approximately constant at early time. As shown in Fig. 5, the third phase grows after $t = 12$.

3.3.4. Energy dissipation

Fig. 6 shows the temporal evolutions of the normalized discrete total energy $\mathcal{E}^h(\phi^n, \psi^n)/\mathcal{E}^h(\phi^0, \psi^0)$ from Eq. (11). The inscribed small figures are the results at the times $t = 4$, 12, and 60. We can see the discrete total energy is decreasing over time. As shown in Fig. 6, all three phases ϕ, ψ, and $1-\phi-\psi$ have similar morphologies and evolution dynamics. To show the robustness of our numerical method, we compare the ratio $\Delta t/h^4$ with the one used in Ref. [1]. In this numerical test, we note that we used a 10^7 times larger ratio than that in Ref. [1].

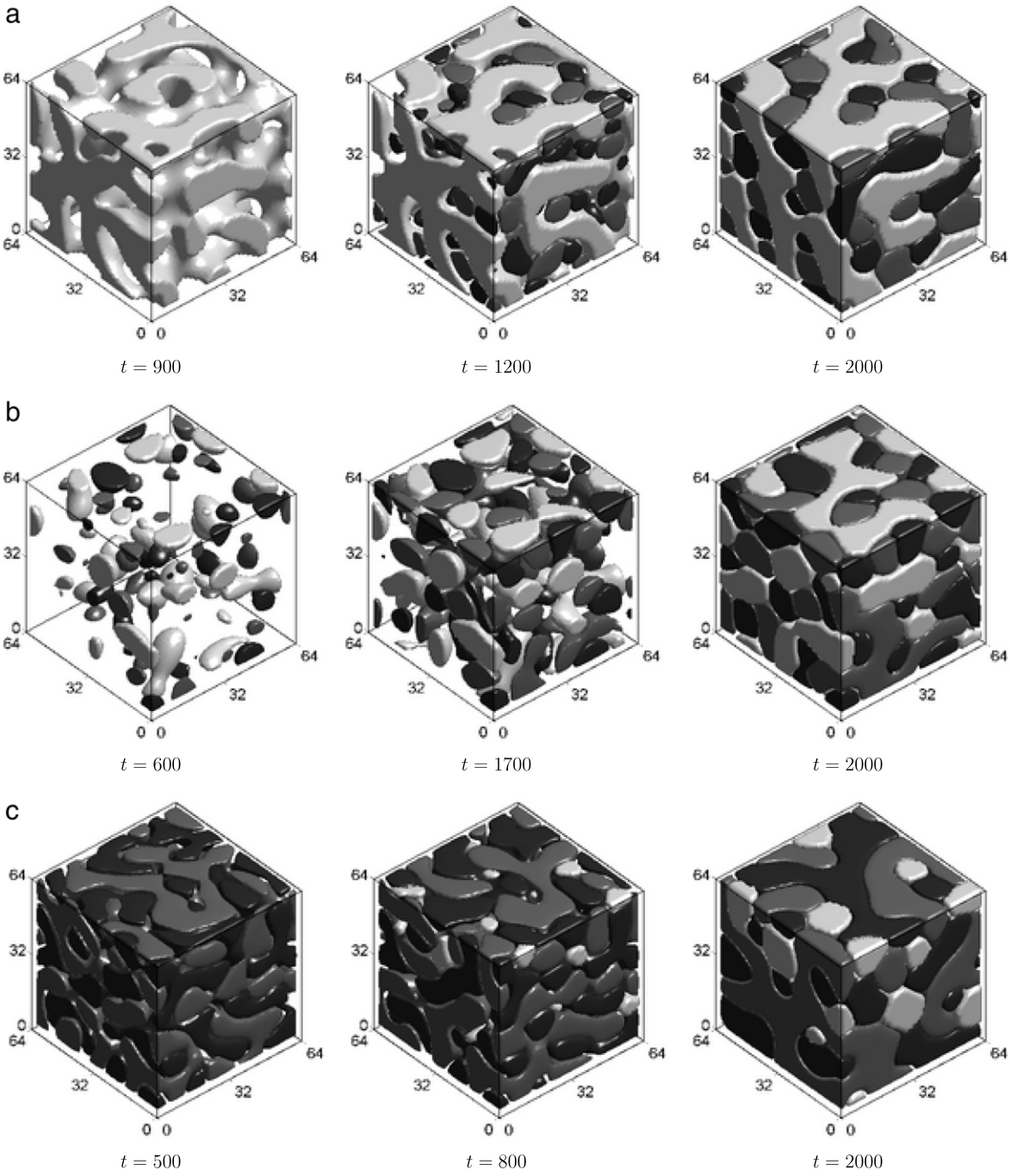

Fig. 10. (a), (b), and (c) are temporal evolutions of a ternary system with average concentrations $(m_1, m_2) = (1/4, 1/4)$, $(m_1, m_2) = (1/3, 1/3)$, and $(m_1, m_2) = (2/5, 2/5)$, respectively. The times are shown below each figure.

3.4. Two-dimensional spinodal decomposition

We examine the two-dimensional spinodal decomposition. The initial conditions are taken to be

$$\phi(x, y, 0) = m_1 + 0.05\ \mathrm{rand}(x, y), \qquad \psi(x, y, 0) = m_2 + 0.05\ \mathrm{rand}(x, y)$$

in $\Omega = (0, 64) \times (0, 64)$. We then take the simulation parameters as $\theta = 0.3,\ \theta_c = 1, \epsilon = \sqrt{0.5},\ h = 1$, and $\Delta t = 1$ up to $T = 3000$. Firstly, we have the numerical test when $(m_1, m_2) = (1/4, 1/4)$. The numerical results are shown in Fig. 7. When the phase $1 - \phi - \psi$ dominates, ϕ and ψ are separated in spatial area where $1 - \phi - \psi$ is not dominant.

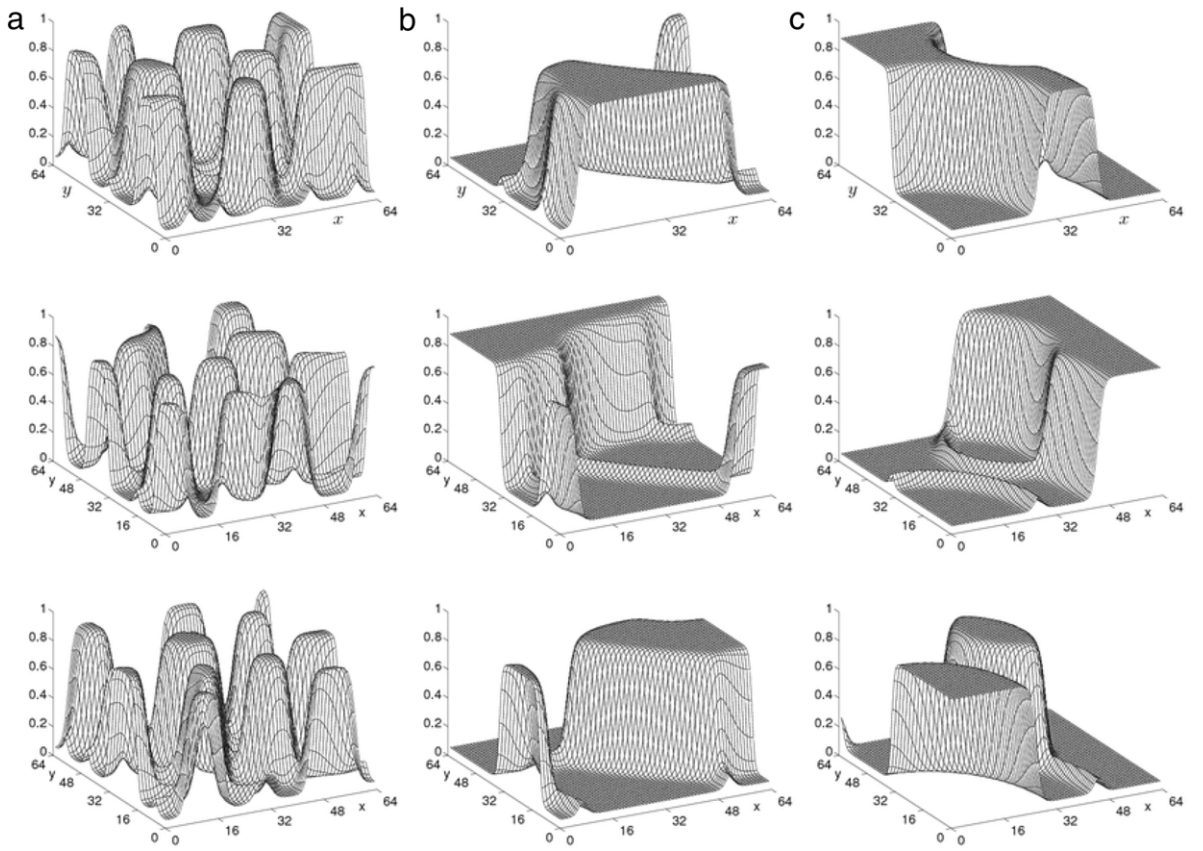

Fig. 11. (a), (b), and (c) are the numerical results after 2000 iterations with time step sizes $\Delta t = 1$, $\Delta t = 100$, and $\Delta t = 10\,000$, respectively. The first, second, and third rows represent ϕ, ψ, and $1 - \phi - \psi$.

Next Fig. 8(a)–(c) represent the time evolutions of ϕ, ψ, and $1 - \phi - \psi$ when $(m_1, m_2) = (1/3, 1/3)$, respectively. As the one-dimensional case, all results at each row have similar morphologies.

In the third test, we set $m_1 = m_2 = 0.4$ which is the point (c) in Fig. 2. The numerical results are presented in Fig. 9. We observe two phases with either ϕ and ψ dominating, while $1 - \phi - \psi$ is approximately constant. After $t = 800$, the third phase of $1 - \phi - \psi$ appears. We note that we used a 10^7 times larger ratio than that in Ref. [1].

3.5. Three-dimensional spinodal decomposition

In this section, we consider a ternary system in three-dimensional domain $\Omega = (0, 64) \times (0, 64) \times (0, 64)$. We take the parameters as $\theta = 0.3$, $\theta_c = 1$, $\epsilon = \sqrt{0.5}$, and $h = 1$. And the initial conditions are

$$\phi(x, y, z, 0) = m_1 + 0.05\ \mathrm{rand}(x, y, z), \qquad \psi(x, y, z, 0) = m_2 + 0.05\ \mathrm{rand}(x, y, z),$$

where the random number $\mathrm{rand}(x, y, z)$ is in $[-1, 1]$ and has zero mean. Fig. 10 shows the numerical results with time step sizes $\Delta t = 1$ up to $t = 2000$. In this figure, the first, second, and third rows represent half isosurface of each component (black: ϕ, dark gray: ψ, and light gray: $1 - \phi - \psi$) at the points $(m_1, m_2) = (1/4, 1/4)$, $(m_1, m_2) = (1/3, 1/3)$, and $(m_1, m_2) = (2/5, 2/5)$, respectively. The times are shown below each figure. In Fig. 10(a), we see that the third phase $1 - \phi - \psi$ (light gray) dominates and the other phases ϕ and ψ grow. As in the second case of the numerical experiments, Fig. 10(b) shows the temporal evolution of the ternary system with spinodal decomposition. And the last example represents two phases with either ϕ or ψ dominating. Then at $t = 800$, we observe that the third phase $1 - \phi - \psi$ grows.

3.6. Robustness of the numerical algorithm

In order to show the robustness of the numerical algorithm, we consider spinodal decomposition with large time step sizes. Initial conditions are set to

$$\phi(x, y, 0) = 1/3 + 0.05\ \mathrm{rand}(x, y), \qquad \psi(x, y, 0) = 1/3 + 0.05\ \mathrm{rand}(x, y)$$

in $\Omega = (0, 64) \times (0, 64)$. We then take the parameters as $\theta = 0.3$, $\theta_c = 1$, $\epsilon = \sqrt{0.5}$, and $h = 1$. Fig. 11(a)–(c) show the numerical results after 1000 iterations with time step sizes $\Delta t = 1$, $\Delta t = 100$, and $\Delta t = 10000$, respectively. In this figure, the first, second, and third rows represent ϕ, ψ, and $1 - \phi - \psi$. These results indicate that the proposed scheme is practically unconditionally stable.

4. Conclusions

In this paper, we proposed a practical numerical method for the ternary CH system with a logarithmic free energy modeling the phase separation of a three-component mixture. The numerical scheme is based on an unconditionally gradient stable finite difference method and is solved by an efficient and accurate multigrid method. We performed a convergence test and a linear stability analysis of the ternary CH equation. We also showed the robustness of our proposed numerical scheme by taking a practically large time step, which is about 10^7 times larger than that of the previous approach. We observed that our numerical solutions are consistent with the exact solutions of linear stability analysis results and are stable with practically large enough time steps.

Acknowledgments

The first author (D. Jeong) was supported by a Korea University Grant. The corresponding author (J.S. Kim) was supported by the National Research Foundation of Korea (NRF) grant funded by the Korea government (MSIP) (NRF-2014R1A2A2A01003683). The authors would like to thank the reviewers for their comments that help improve the manuscript.

References

[1] M.I.M. Copetti, Math. Comput. Simul. 52 (2000) 41.
[2] D.J. Eyre, SIAM J. Appl. Math. 53 (1993) 1686.
[3] D.D. Fontaine, A computer simulation of the evolution of coherent composition variations in solid solutions (Ph.D. Thesis), Northwestern University, 1967.
[4] J.E. Morral, J.W. Cahn, Acta Metall. 19 (1971) 1037.
[5] J.W. Cahn, J.E. Hilliard, J. Chem. Phys. 28 (1958) 258.
[6] D. Lee, J.-Y. Huh, D. Jeong, J.M. Shin, A. Yun, J. Kim, Comput. Mater. Sci. 81 (2014) 216.
[7] H. Garcke, B. Nestler, B. Stoth, Physica D 115 (1998) 87.
[8] J.F. Blowey, M.I.M. Copetti, C.M. Elliott, IMA J. Numer. Anal. 16 (1996) 111.
[9] P. Boyanova, M. Neytcheva, Comput. Math. Appl. 67 (2014) 106.
[10] F. Guillén-González, G. Tierra, Comput. Math. Appl. 68 (2014) 821.
[11] F. Boyer, S. Minjeaud, ESAIM: Math. Model. Numer. Anal. 45 (2011) 697.
[12] H.G. Lee, J.W. Choi, J. Kim, Physica A 391 (2012) 1009.
[13] S. Minjeaud, Numer. Methods Partial Differential Equations 29 (2013) 584.
[14] F. Boyer, S. Minjeaud, Math. Models Methods Appl. Sci. 24 (2014) 2885.
[15] J.W. Barrett, J.F. Blowey, Numer. Math. 72 (1995) 1.
[16] J.W. Barrett, J.F. Blowey, IMA J. Numer. Anal. 16 (1996) 257.
[17] D.J. Eyre, Unconditionally gradient stable time marching the Cahn–Hilliard equation, in: Computational and Mathematical Models of Microstructural Evolution, The Material Research Society, Warrendale, US, 1998.
[18] C.M. Elliott, A.M. Stuart, SIAM J. Numer. Anal. 30 (1993) 1622.
[19] J.W. Barrett, J.F. Blowey, Numer. Math. 77 (1997) 1.
[20] J.W. Barrett, J.F. Blowey, IMA J. Numer. Anal. 18 (1998) 287.
[21] J. Kim, Commun. Nonlinear Sci. Numer. Simul. 12 (2007) 1560.
[22] W.L. Briggs, V. Henson, S. McComick, A Multigrid Tutorial, SIAM, US, 2000.
[23] U. Trottenberg, C.W. Oosterlee, A. Schuller, Multigrid, Academic Press, US, 2000.